

## Fabrication of high-durability superhydrophobic coatings based on dual-sized SiC particles

Z. Y. Xue<sup>a</sup>, C. Q. Li<sup>a,\*</sup>, H. W. Niu<sup>a</sup>, J. F. Ou<sup>a</sup>, F. J. Wang<sup>a</sup>, X. Z. Fang<sup>a</sup>, W. Li<sup>a</sup>,  
A. Amirfazli<sup>b</sup>

<sup>a</sup>*School of Materials Engineering, Jiangsu University of Technology, Changzhou 213001, China*

<sup>b</sup>*Department of Mechanical Engineering, York University, Toronto ON M3J 1P3, Canada*

In recent years, inspired by “biomimicry”, superhydrophobic surfaces have gained significant attention. Superhydrophobic surfaces demonstrate notable advantages in addressing interfacial issues, and superhydrophobic coatings exhibit excellent waterproofness, anti-fouling, self-cleaning, anti-corrosion, and additional capabilities, making them promising next-generation waterproof materials. However, the complex preparation process, coupled with poor wear resistance and environmental durability, severely limits their practical applications. Therefore, this article started from simplifying the preparation process and improving the durability of the coatings. Epoxy resin (E51) was used as the film-forming material, and carbon nanotubes (CNTs) and dual-sized SiC particles (nano-SiC and micro-SiC) were used as the fillers. Room temperature vulcanized silicone rubber (RTV) was used as a binder interacting with epoxy resin to promote the interface interaction between the fillers and the polymers. This process resulted in the successful preparation of superhydrophobic coatings with outstanding comprehensive performance. When the ratio of  $\mu$ -SiC to n-SiC was 1:1, the prepared coating exhibited the best superhydrophobic properties with a water contact angle (WCA) of 167.4° and a sliding angle (SA) of 4.6°. Even after undergoing severe mechanical tests, such as sandpaper abrasion for 1000 cycles, sand impact for 100 cycles, cross-cut test, and tape-peeling for 70 cycles, the coatings still maintained their non-wetting Cassie-Baxter state. Furthermore, even after immersion in strong acid, strong alkali and 3.5 wt% NaCl solutions for 6 days, keeping at 500 °C for 2 hours, and exposure to ultraviolet for 6 days, the coatings still exhibited excellent superhydrophobicity. This suggested that the prepared coating had excellent chemical stability and high-temperature resistance. In addition, the superhydrophobic coating exhibited exceptional capabilities in self-cleaning, anti-corrosion, anti-icing, and de-icing properties. Furthermore, this coating, applicable to diverse substrates including board, steel, paper, and glass, demonstrated an impressive water contact angle (WCA) and sliding angle (SA). The spraying method offers the benefits of simplicity and cost-effectiveness. This is poised to significantly broaden its practical applications in various fields, including construction, transportation, and the chemical industry.

(Received December 27, 2023; Accepted March 7, 2024)

*Keywords:* Superhydrophobic coatings, Nanoparticles, Durability, Bio-inspired

### 1. Introduction

Inspired by lotus leaves, superhydrophobic coatings are typically characterized by a water contact angle (WCA) above 150° and a sliding angle (SA) below 10°<sup>[1]</sup>. These surfaces find diverse applications in various fields, including self-cleaning<sup>[2],[3]</sup>, anti-bioadhesion<sup>[4],[5]</sup>, oil-water separation<sup>[6],[7]</sup>, anti-icing<sup>[8],[9]</sup>, and non-loss liquid transportation<sup>[10]</sup>. Their unique superhydrophobic properties also play a crucial role in reducing the corrosion of metal materials in environments such as the ocean and soil<sup>[11],[12]</sup>.

\* Corresponding author: xzy17365381209@163.com

<https://doi.org/10.15251/DJNB.2024.191.383>

These have garnered widespread attention in both academia and industry<sup>[13]</sup>. Through the exploration of superhydrophobic surfaces in nature and the analysis of the superhydrophobic theoretical model, researchers have discovered that the superhydrophobicity of these surfaces relies on the synergistic effect of hierarchical rough structure and low surface energy<sup>[14],[15]</sup>. Consequently, various physical and chemical approaches have been devised to prepare superhydrophobic coatings, including etching<sup>[16],[17]</sup>, sol-gel<sup>[18]</sup>, templating methods<sup>[19]</sup>, and so on. However, many of these methods involve complex synthesis processes, specialized equipments, or expensive raw materials, limiting the industrial applications of superhydrophobic surfaces. In comparison, the use of the spray-coating approach to prepare composite coatings has many advantages such as universality, cost-effectiveness, strong operability, and enabling large-scale production. Sun et al.<sup>[20]</sup> achieved the successful preparation of a superhydrophobic coating characterized by exceptional mechanical stability through a blend of nano-SiO<sub>2</sub>, PFDTES, and epoxy resin using the spray-coating method. The water contact angle of the coating reached 152.4°, with a minimal contact angle of 2.6°, and it exhibited stability over 40 cycles of abrasion. More importantly, it demonstrated strong corrosion resistance. However, most superhydrophobic coatings with hierarchical rough structure are susceptible to surface fragility. After inevitable wear or abrasion, the superhydrophobicity of the coatings can significantly reduce or even eliminate its superhydrophobic properties. Therefore, the preparation of a series of superhydrophobic surfaces with excellent durability is crucial for their practical application.

Specifically, the durability of superhydrophobic coatings is primarily influenced by factors such as the abrasion resistance of surface micro-nano structures, adhesion to the substrate, and chemical functional groups<sup>[21],[22]</sup>. Therefore, preparing durable superhydrophobic coatings is a complex challenge that requires innovative preparation methods and suitable materials. Some researches indicated that the superhydrophobic surface formed by two hard wear-resistant particles with dual-sized (microscale and nanoscale) exhibit excellent superhydrophobic properties even after wear or abrasion, opening up a new research area for the preparation of stable superhydrophobic surfaces<sup>[23]</sup>. Microparticles and nanoparticles can construct the necessary micro-nano rough structures for superhydrophobic surfaces, with nanostructures providing wetting properties and other key functionalities, while microstructures primarily serves a protective function<sup>[24]</sup>, which are essential for achieving the superhydrophobicity of the coating. Zhu et al.<sup>[25]</sup> prepared a highly stable superhydrophobic coating by spraying a mixture of two modified particles (diatomite microparticles and SiO<sub>2</sub> nanoparticles) on the epoxy resin layer. Thanks to the micro-nano rough structure, the water repellency of the coatings still retained after the 1500g sand impact. Xiao et al.<sup>[26]</sup> fabricated a superhydrophobic coating with excellent mechanical stability using MoS<sub>2</sub> or WS<sub>2</sub> microparticles as solid lubricants and SiO<sub>2</sub> nanoparticles as fillers combined with PDMS using a one-step spray method. When MoS<sub>2</sub> or WS<sub>2</sub> microparticles were mixed with SiO<sub>2</sub> nanoparticles, it was easy to form micro-nano hierarchical rough structure, which made the coatings superhydrophobic. Furthermore, the addition of microparticles reduced the friction coefficient of the coatings, thus improving the mechanical property of the coatings. These innovative studies have advanced the development of durable superhydrophobic coatings. However, most durable superhydrophobic coatings are single-functional and may not be suitable for specific scenarios. Therefore, there is a need to prepare a multifunctional durable superhydrophobic coating to enable its use in a wider range of applications.

Serving as an interface enhancer between the substrates and the coatings, epoxy resin demonstrates remarkable adhesion, mechanical and chemical stability. However, its high rigidity and brittleness pose challenges when used independently for coating preparation<sup>[27]</sup>. Additionally, its hydrophobicity and high-temperature stability are limited, hindering the widespread use of epoxy resin in the preparation of durable superhydrophobic coatings. Therefore, improving and optimizing the application performance of epoxy resin can be achieved by adding micro-nanoparticles with large specific surface area and wear-resistant. In the process of coating preparation, epoxy resin has been widely utilized as a polymer adhesive, blended with micro-nanoparticles to establish a hierarchical rough structure on the coating surface, thereby improving the durability performance of the coating<sup>[28],[29]</sup>. SiC, known for its advantages such as good wear resistance, chemical stability, high-temperature stability, and non-toxic and harmless<sup>[30]</sup>, is often used to construct micro-nano rough structures on the surface of the coatings. Considering wear resistance, high-temperature stability, and economy, SiC particles are suitable nanofillers for polymers. When these particles are incorporated into epoxy resin, a strong interface effect is

generated, enhancing the adhesion between epoxy resin and SiC particles. This interface effect contributes to improve mechanical properties of epoxy resin, leading to an overall enhancement in the strength and toughness of the coatings<sup>[31]</sup>. Additionally, carbon nanotubes (CNTs) with a distinctive intertwined structure are often incorporated into polymers to prepare superhydrophobic coatings with excellent mechanical stability, owing to their outstanding physical, thermal, and electrical properties<sup>[32]</sup>. However, the limited interaction at the interface between CNTs and the polymer hinders the establishment of effective bonding, limiting further enhancement of the strength and toughness of the coatings. To further improve the interface interaction between micro-nanomaterials and polymers, room temperature vulcanized silicone rubber (RTV) with inorganic main chains (Si-O) and organic side chains (-CH<sub>3</sub>) was introduced. RTV is a hydrophobic elastic silicone rubber known for its excellent wear resistance, water repellency, and adhesion<sup>[33],[34],[35]</sup>. It is often added as an organic component to coatings to enhance the hydrophobicity of the coating surface and the interface stability between the coatings and the substrates. The Si-O groups in RTV can engage with the hydroxyl and amino groups present in epoxy resin, establishing hydrogen bonds that enhance the interfacial interaction between micro-nanoparticles and polymers. This makes micro-nanoparticles firmly attached to the substrate.

In this study, we employed one-step spraying method to prepare a SiC&CNTs/EP/POTS/RTV superhydrophobic coating with outstanding durability at room temperature. We investigated the effect of the mass ratio of nano-SiC (n-SiC) and micro-SiC ( $\mu$ -SiC) on the superhydrophobicity of the coatings. The wetting property, morphology, chemical composition, self-cleaning ability, durability, chemical stability, de-icing, and anti-icing performances of the coatings surface were tested and analyzed. The prepared coatings can be applied to various substrate surfaces and exhibited excellent durability under sandpaper abrasion, sand impact, tape-peeling, and cross-cut tests. Notably, the coating maintained its superhydrophobicity even when exposed to harsh environments such as immersion in acid, alkali, salt solutions, and ultraviolet. Furthermore, the coatings demonstrated outstanding corrosion resistance, anti-icing, and de-icing performances. Therefore, this spray-coated superhydrophobic coating hold promising potential for widespread applications in different fields such as construction, transportation, and chemicals.

## 2. Materials and methods

### 2.1. Experimental materials

Epoxy resin (EP, E51), curing agent (D230), butyl acetate, tetraethyl orthosilicate (TEOS), and dibutyltin dilaurate (DBTDL) were all Kunshan Electronic Materials Co., Ltd. Multi-walled carbon nanotubes (CNTs, diameter 8-15nm, length 3-12 $\mu$ m) were purchased from Nanjing Genesis Chemical Auxiliary. Co., Ltd. Perfluorooctyltriethoxysilane-(C<sub>8</sub>F<sub>13</sub>H<sub>4</sub>Si(OC<sub>2</sub>H<sub>5</sub>)<sub>3</sub>, POTS,) was purchased from Urn River Chemical Reagent Co., Ltd. Room temperature vulcanized silicone rubber (RTV, viscosity of 10000 cP) was purchased from Jinan Duoweiqiao Chemical Co. Ltd. Nano-SiC (50nm) and micro-SiC (5 $\mu$ m) particles were purchased from Shanghai Aladdin Reagent Co., Ltd. Aluminum sheets were purchased from Shandong Shengxin Technology Co., Ltd.

### 2.2. Preparation of bare aluminum substrates

The bare aluminum sheets were polished in different directions with 400-mesh sandpaper . Subsequently, the aluminum sheets underwent ultrasonic cleaning with anhydrous ethanol for 30 minutes to eliminate any remaining impurities on the surface. Finally, the aluminum sheets were thoroughly washed with deionized water for 2 times and dried for later use.

### 2.3. Preparation of superhydrophobic composite coatings

As shown in Fig. 1,  $\mu$ -SiC (1g) and n-SiC (1g) were dissolved in butyl acetate (15g) and magnetically stirred at room temperature for 2 h, followed by ultrasonic oscillation for 30 min to prevent particles aggregation. Then POTS (0.2g), E51 (2.7g), and D230 (0.9g) were added, and continued the stirring process for 2 h. Finally, CNTs (0.1g), RTV (0.8g), TEOS (0.08g), and DBTDL (0.008g) were introduced into the mixture, and the stirring continued for 1 h. The obtained solution was spray-coated on cleaned aluminum sheets using a pressure of 0.5 MPa. The

spray gun was perpendicular to the aluminum substrates and the spraying time was 30 s. The prepared coatings were cured at 60 °C for 6h, resulting in the formation of superhydrophobic SiC&CNTs/EP/POTS/RTV coating. The preparation process is illustrated in Fig. 1.

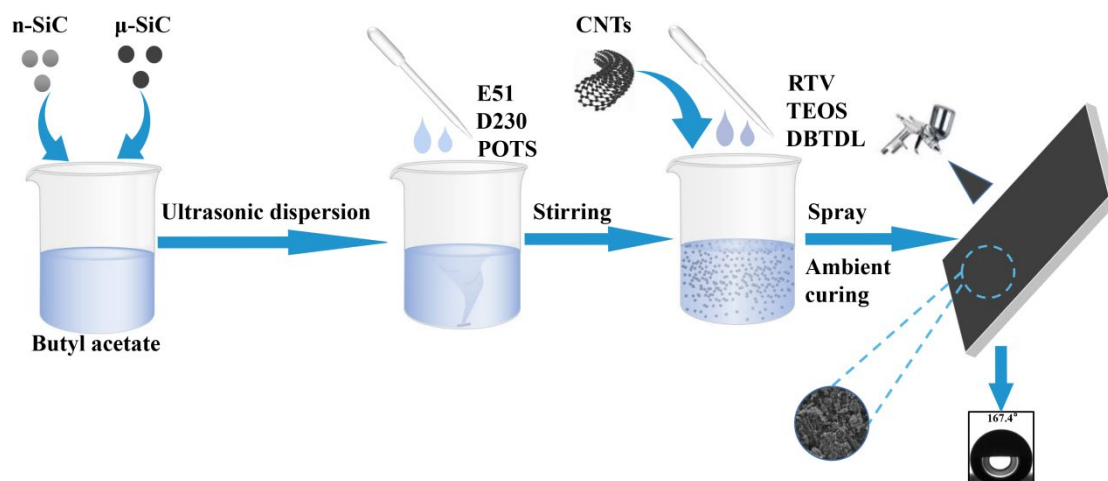


Fig. 1. Diagram of superhydrophobic SiC&CNTs/EP/POTS/RTV coating preparation.

#### 2.4. Characterization of superhydrophobic composite coatings

After completing the preparation of the coating, the morphology and physical structure of the superhydrophobic coating were analyzed using scanning electron microscopy (SEM, QUANTA Q400, FEI Corporation, USA). The specific elements present in the coatings and their respective concentrations were analyzed by using an energy dispersive spectrometer (EDS, Oxford Instruments Technology Ltd).

#### 2.5. Wettability and anti-fouling performance tests

The WCA and SA of the samples were measured using a contact angle meyer (Krüss, DSA 30). A fixed volume of 10  $\mu$ L water droplet was used, with five points selected from different areas of the coatings. The final test value was determined by averaging these measurements.

Sand was used as a simulated pollutant and evenly spread on the superhydrophobic coating (the coated substrate was tilted at 45 °). The residual degree of the sand on the coating was observed<sup>[36]</sup>.

#### 2.6. Durability test

The abrasion test involved placing the coating face down on a 1000-mesh sandpaper with a load of 100 g and it was horizontally moved uniformly on the 1000-mesh sandpaper at a speed of 0.05m/s. The coating surface was downward and made contact with the sandpaper. The Variation of surface wettability were recorded after each 1 m movement on the sandpaper. For the sand impact test, 150g sand fell from a height of 40 cm at a certain speed, impacting the inclined coating sample (the coated substrate was tilted at 45 °). The variation of surface wettability were measured after every 10 impacts. For the cross-cut test, a grid of multiple 2mm×2mm squares was drawn on the coating surface with a grid cutter, adhering them to the grid surface with 3M tape and pressed repeatedly with fingers. The tape was peeled off smoothly and repeated several times at a certain angle until no debris remained on the tape.

Adhesion test was conducted on the samples with reference to the “Paint and Varnishes-Cross-Cut Test” (GB/T 9286-2021/ISO 2409:2020). 3M tape with a load of 100g was attached to the coating surface, and the load was rolled back and forth on the tape surface. The tape was then peeled off smoothly. The variation of surface wettability were measured after every 10 peels.

The coating underwent immersion in acidic solution (pH=2), alkaline solution (pH=14), and 3.5 wt% NaCl solution. After soaking for a certain period, the variation of surface wettability were measured<sup>[37]</sup>. For assessing the ultraviolet resistance, the samples were exposed to ultraviolet.

After a certain period of irradiation, the variation of surface wettability were measured and recorded<sup>[37]</sup>. In the high-temperature test, the coating was placed in a muffle furnace (ksl-1400×) and kept at different high temperatures for a certain time. Subsequently, the variation of surface wettability were measured and recorded<sup>[38]</sup>. In the corrosion resistance test, the electrochemical workstation (GAMRY Reference 3000) was used to obtain the kinetic potential polarization curve.

### 2.7. Anti-icing and de-icing performance tests

For the anti-icing performance test, the samples were placed inside a temperature control chamber (TC 40, Kruss Germany) set to  $-30\text{ }^{\circ}\text{C}$  and  $35 \pm 5\%$  relative humidity. Then the freezing time of water droplets with a volume of  $10\text{ }\mu\text{L}$  on the surface of the bare aluminum sheet and the coating at  $-10\text{ }^{\circ}\text{C}$  were observed and recorded. For the de-icing performance test, the coating and bare aluminum sheet were placed in a refrigeration unit (MC711, SHIPAC, China) at  $-30\text{ }^{\circ}\text{C}$ , allowing a layer of ice approximately 2 mm thick to form on their surfaces. Subsequently, the coating and the bare aluminum sheet were placed under a xenon lamp (MC711, SHIPAC, China) at an ambient temperature of  $14 \pm 0.5\text{ }^{\circ}\text{C}$ . The melting time of the ice on the bare aluminum sheet and the coating were observed and recorded.

## 3. Results and discussion

### 3.1. Characterization of surface morphology and chemical composition

As shown in Fig. 2a, b, the SiC&CNTs/EP/POTS/RTV superhydrophobic coating was characterized using SEM. From the SEM images at different magnifications, a continuous dense EP+RTV layer can be observed on the coating surface, which was composed of micro-nano protrusions and pits. There were few threads between these protrusions, and many small particles adhered to the surface of the protrusions. Simultaneously, numerous holes of various shapes were found between these protrusions, which can capture a considerable amount of air. When the sample is immersed in the corrosive solution, the trapped air forms a dense air layer, blocking the erosion of the corrosive solution.

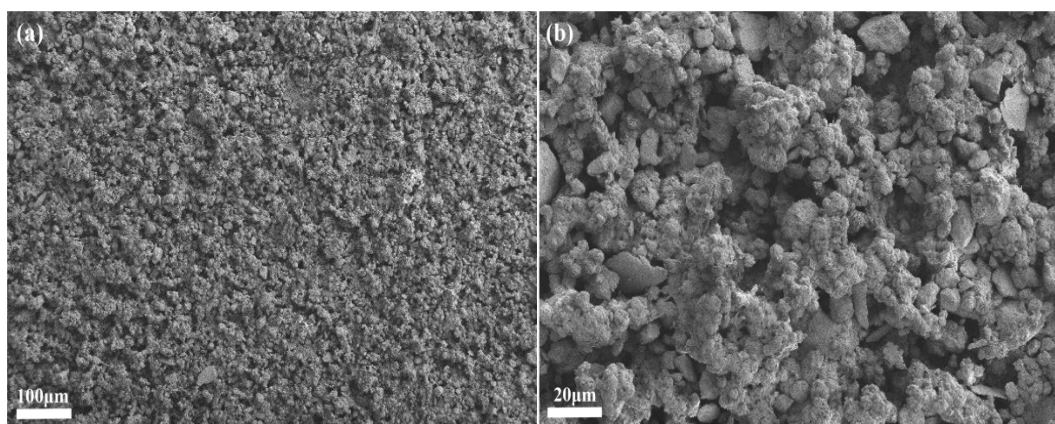


Fig. 2. SEM images of superhydrophobic SiC&CNTs/EP/POTS/RTV coatings

The hierarchical rough structure on the coating surface is the crucial factor to achieving the superhydrophobicity of the coating, and ensures a low contact area and penetration depth of the droplets on the coating<sup>[39]</sup>. The combination of hydrophobic POTS and RTV imparts a lower surface energy to the coating. The synergy of low surface energy and hierarchically rough structure are the two essential conditions required for constructing a superhydrophobic coating.

EDS maps and spectrum in Fig.3 revealed a uniform distribution of a large number of elements such as C, Si, and O on the coating surface, with weight percentages (wt%) of 57.0%, 30.4%, and 12.6%, respectively. C, Si, and O are the main constituent elements of SiC and CNTs, indicating the successful attachment of SiC and CNTs to the substrate.

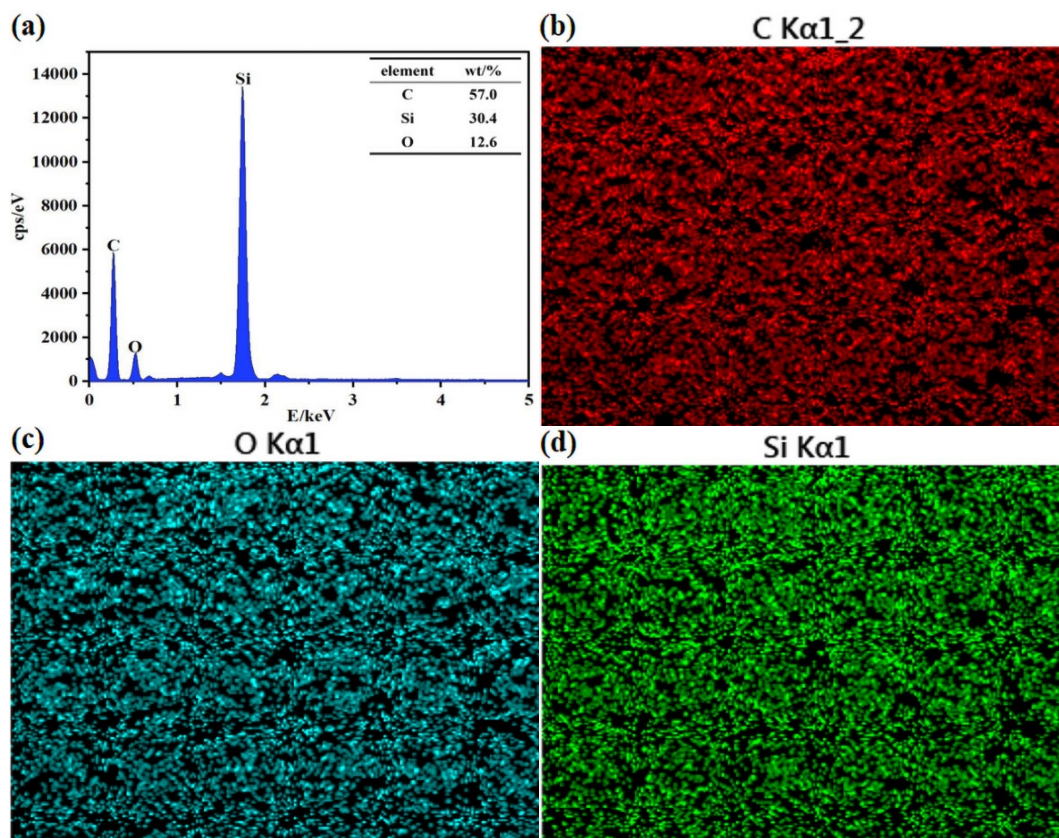


Fig. 3. Elemental composition and distribution of superhydrophobic SiC&CNTs/EP/POTS/RTV coatings.

To investigate the influence of the mass ratio of  $\mu$ -SiC to n-SiC on the wettability of the coating, we prepared four additional samples with different ratios of  $\mu$ -SiC to n-SiC, as shown in Fig. 4a-d. The colors of the coatings are slightly different. As shown in Fig. 3e, when only  $\mu$ -SiC (1g) were added, there were some protrusions and pits on the surface, with a certain degree of roughness. However, the particles aggregated excessively and were tightly encapsulated by epoxy resin. Additionally, the surface energy of epoxy resin is significantly higher than that of the modified micro-nanoparticles. Therefore, achieving superhydrophobicity for the coating solely based on surface roughness is challenging. The measured water contact angle (WCA) was only  $135.2^\circ$ . When n-SiC (1g) was added, the number of protuberances and surface micro/nano pits gradually increases, creating numerous pores on the coating surface. These pores can capture air, forming an air layer that imparts excellent hydrophobicity to the coating. However, as shown in Fig. 4f, when both  $\mu$ -SiC (1g) and n-SiC (2g) were added, the pore size of the coating surface was relatively small. This phenomenon could be attributed to the substantial presence of epoxy resin covering the pores, leading to a decrease in the hydrophobicity of the coating. Consequently, the measured water contact angle (WCA) was  $153.1^\circ$ . As depicted in Fig. 4g., when  $\mu$ -SiC (2g) and n-SiC (1g) were added, the number of pores and protuberances on the coating surface was reduced, and a significant amount of micro-nano particles covered the pores, resulting in lower roughness of the coating. Therefore, the hydrophobicity was not ideal, and the measured WCA was lower. In Fig. 4h., when only n-SiC (1g) was added, it can be observed that circular protuberances of micrometer scale appeared on the surface. Many nanoparticles adhered to the protuberance surface, forming micro-nano porous structures. It contributed to the excellent hydrophobic performance of the coating, with a measured WCA of  $155.2^\circ$ .

Here, we explored how the mass ratio of  $\mu$ -SiC to n-SiC affected the surface morphology and wettability of the coating. The ratio of 1:1 was determined to achieve the optimal superhydrophobicity. Therefore, we will proceed to test various properties of the coating prepared with this ratio.

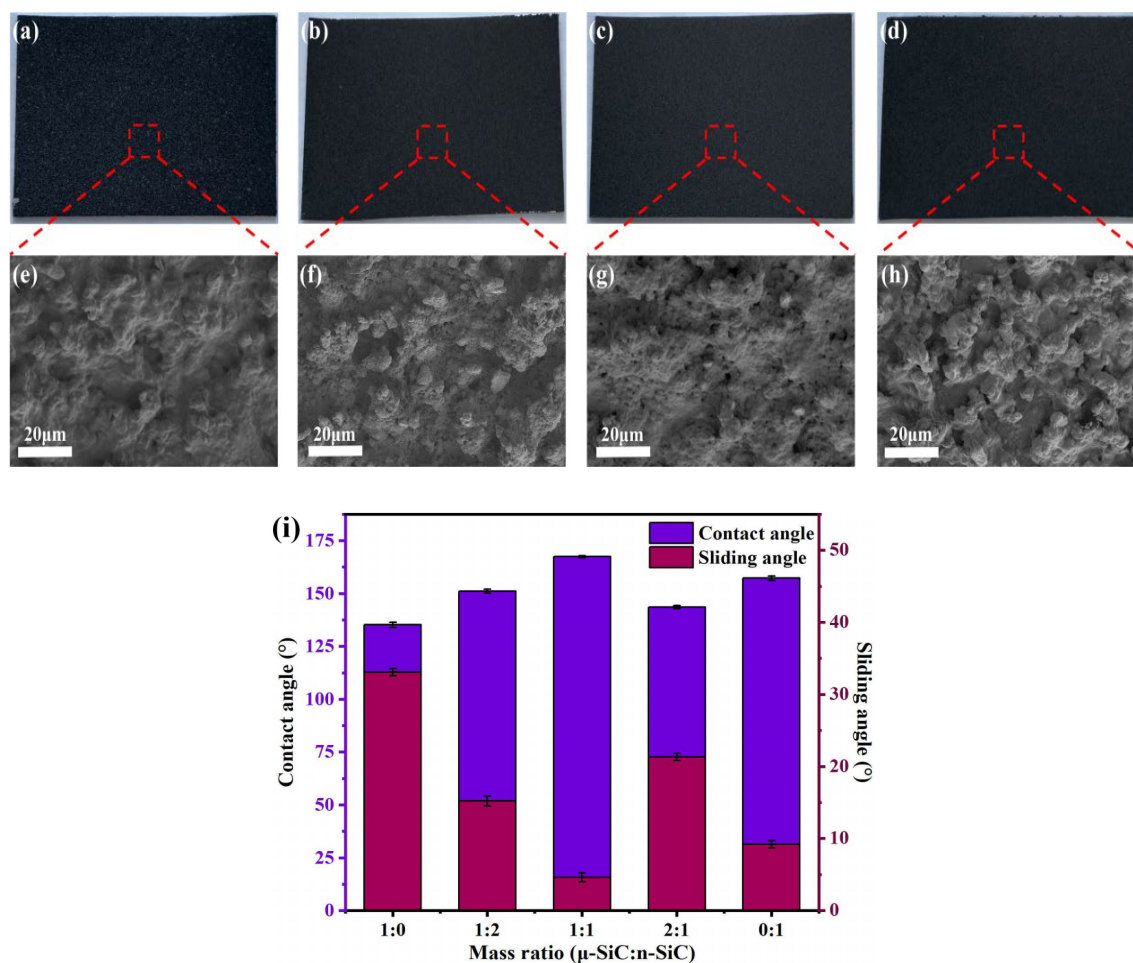


Fig. 4. Optical photos of  $\mu$ -SiC/n-SiC 1:0(a),  $\mu$ -SiC/n-SiC 1:2(b),  $\mu$ -SiC/n-SiC 2:1(c) and  $\mu$ -SiC/n-SiC 0:1(d) coatings. SEM images of  $\mu$ -SiC/n-SiC 1:0(e),  $\mu$ -SiC/n-SiC 2:1(f),  $\mu$ -SiC/n-SiC 0:1(g) and  $\mu$ -SiC/n-SiC 1:2(h) coatings. (i) Variation of the surface wettability of different ratios of  $\mu$ -SiC/n-SiC coatings.

### 3.2. Anti-fouling and self-cleaning performance tests

Coatings are frequently susceptible to contamination by various pollutants when applied in different fields. Solid and liquid contaminants tend to adhere to hydrophilic surfaces. As shown in Fig. 5, various liquid contaminants such as coffee, mud, juice, paint, and soy sauce were dropped onto the coating as pollution media. The anti-fouling ability was evaluated by observing the shapes of liquid contaminants on the superhydrophobic coating. The droplets on the coating surface all assumed a spherical shape. This suggested that the superhydrophobic coating exhibited outstanding resistance to liquid contaminants, showcasing excellent anti-fouling performance. The excellent anti-fouling performance can be attributed to its hydrophobicity and extremely low interfacial forces. Simultaneously, as shown in Fig. 5b-e, dropping water droplets onto the surfaces of various substrates sprayed with the superhydrophobic coating, respectively. It could be observed that the water droplets rapidly rolled off the coating surface in a spherical shape without leaving any traces. This indicated that the superhydrophobic coating could be applied to various substrates, and its superhydrophobic performance was excellent.

The self-cleaning ability of superhydrophobic coatings is also essential for their practical applications. When there was sand on the coating surface, water droplets rapidly rolled off the coating surface, carrying away some of the sand. The self-cleaning performance was evaluated by observing the extent of residual sand on the superhydrophobic surface, as shown in Fig. 5f and g. What can be observed was that a clean path appeared on the superhydrophobic surface. As the

number of falling water droplets increases, all the sand and debris on the coating slide off with the water droplets. This indicated that the superhydrophobic coating exhibited excellent self-cleaning performance. Fig. 5h illustrated the schematic diagram of the self-cleaning process. The stable air layer caused water droplets to tend to roll downward and carry away contaminants deposited on the surface.

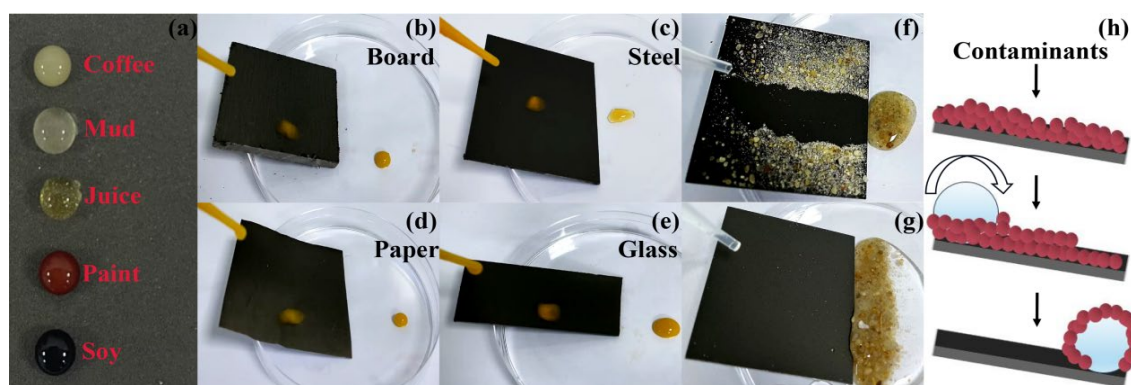


Fig. 5. (a) Water droplet images of different solutions on superhydrophobic coatings, (b) (c) (d) (e) are a hydrophobicity test for superhydrophobic coatings based on different substrates, (f) (g) are a self-cleaning test for superhydrophobic coatings contaminated with sand, (h) is a schematic diagram of the self-cleaning process of superhydrophobic coatings.

### 3.3. Durability test

Superhydrophobic coatings are easily damaged by external forces during the process of outdoor practical applications. For many coatings developed to date, even slight friction or finger pressing can disrupt the hierarchical rough structure of the superhydrophobic surface. Therefore, the durability of superhydrophobic coatings is one of the important criteria for evaluating coating performance<sup>[40]</sup>. In this study, we tested the durability and adhesion of the coating through sandpaper abrasion, sand impact, cross-cut, and tape-peeling tests.

#### 3.3.1. Wear resistance and impact resistance tests

The wear resistance of the coating was assessed through sandpaper abrasion tests. As shown in Fig. 6b, the sandpaper abrasion had a significant impact on the wettability of the coating. After 1000 abrasion cycles, the WCA decreased from  $167.4 \pm 1.5^\circ$  to  $151.1 \pm 1.6^\circ$ , and the SA increased from  $4.6 \pm 0.3^\circ$  to  $17.5 \pm 0.4^\circ$ , indicating a transition from superhydrophobic to hydrophobic. When the abrasion cycles reached 1400, the WCA further decreased to  $135.4 \pm 1.6^\circ$ , and the SA further increased to  $30.9 \pm 0.4^\circ$ , indicating the loss of superhydrophobicity. We believe that although the rough structure was continuously damaged, this structure hindered the wear process of the EP+RTV layer by friction, dissipating most of the energy from the abrasive particles and minimizing harm to the EP+RTV layer by friction. When the abrasion reached 1100 cycles, the coating transitioned from superhydrophobic to hydrophobic. The maintenance of superhydrophobicity became challenging. Despite this, the coating still demonstrated excellent wear resistance.

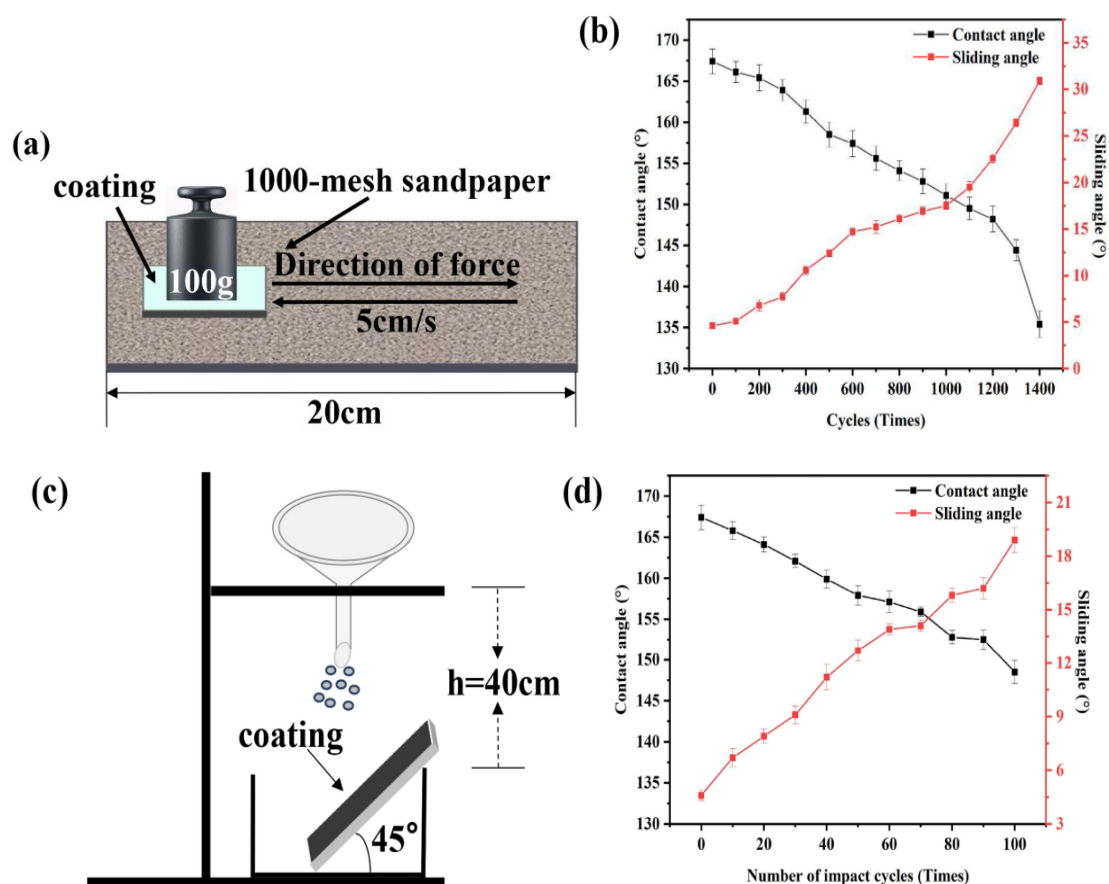


Fig. 6. (a) Schematic diagram of sandpaper abrasion, (b) Variation of surface wettability against wear cycles, (c) Schematic diagram of sand impact, (d) Variation of surface wettability against sand impact cycles.

In addition, gravel impact tests are commonly employed to simulate the wind-blown sand impact in real-world environments, assessing the impact resistance of superhydrophobic coatings. Fig. 6c illustrated the schematic diagram of the sand impact process. Continuous sand impact resulted in the wearing out of certain protrusions, causing the collapse of micro-nano hierarchical structures and making it difficult to maintain integrity.

From Fig. 6d, it could be seen that continuous sand impact caused the hierarchical rough structure of the superhydrophobic coating to be difficult to maintain integrity. Sand may fill into the grooves on the coating surface, weakening the roughness of the surface. As a result, WCA continuously decreased, and the SA continuously increased. After undergoing 100 cycles of sand impact, the WCA experienced a significant decrease, dropping from  $167.4 \pm 1.5^\circ$  to  $148.5 \pm 1.4^\circ$ , and the SA increased from  $4.6 \pm 0.3^\circ$  to  $18.9 \pm 0.7^\circ$ , indicating a substantial increase. However, the coating still maintained good hydrophobicity. This result confirmed the excellent impact resistance of the superhydrophobic coating, making it capable of withstanding the impact of wind and sand in real environmental conditions.

### 3.3.2. Adhesion Test

Good adhesion between the coatings and the substrates is crucial for its broad application prospects in real life. We evaluated the adhesion of the coating through standard cross-cut tape tests and tape-peeling tests.

Following the standard of “Paint and Varnishes-Cross-cut test” (GB/T 9286-2021/ISO 2409:2020)<sup>[41]</sup>, the prepared superhydrophobic coating were cut into multiple squares. As shown in Fig. 7a, the cut edges of the samples were completely smooth, and the grids were intact. There

were no apparent gaps between the grids, with minimal powder observed. Simultaneously, as observed in Fig. 7c, after cross-cut test, only a small amount of powder peeled off from the coating surface and the peel-off areas were significantly less than 5%. Therefore, comparing with the international standard in Fig. 7d, it could be concluded that the adhesion of the superhydrophobic coating reached the highest grade (Grade 1), indicating excellent adhesion of the superhydrophobic coating. Moreover, it was easy to observe that the coating still exhibits excellent hydrophobicity after the cross-cut test, and water droplets did not adhere to the coating. The test indicated that coating were firmly attached to the substrate surface.

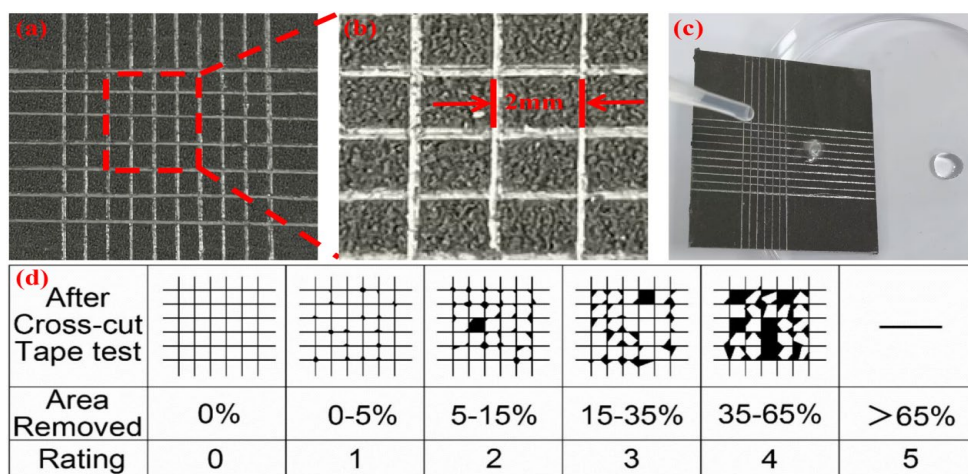


Fig. 7. (a) (b) are a adhesion test of superhydrophobic coatings; (c) is the photo of the wettability test of the coating after the cross-cut test; (d) is GB/T 9286-2021/ISO 2409:2020.

In addition, we also conducted a tape peel test to assess the adhesion of coating. Fig. 8a,b illustrated the schematic diagram of the tape-peeling test and the changes in the surface wettability after different tape-peeling cycles. Observations revealed that with an increase in peel cycles, WCA slightly decreased, and SA gradually increased. After 70 tape-peeling cycles, the WCA can still be maintained above  $150^\circ$ , and the SA gradually increases to  $17.4^\circ$ . The coating transitioned from superhydrophobic to hydrophobic, but it still maintained excellent hydrophobicity. These results indicated that the prepared coating exhibited outstanding adhesion and anti-stripping ability. The combination of chemical bonds between EP and RTV enhances the interfacial interaction between micro-nanomaterials and polymers. As a result, micro-nanoparticles could be firmly attached to the substrate and were not easily peeled off from the substrate under external forces.

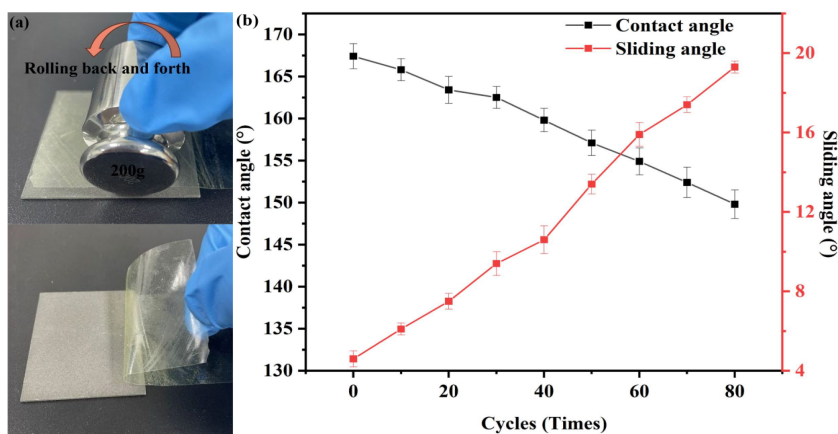


Fig. 8. (a) is the photo of tape-peeling; (b) Variation of surface wettability against tape peel cycles for the coatings.

### 3.4. Chemical and high-temperature stability tests

In the chemical stability test, we exposed the coatings to acidic solution (pH=2), alkaline solution (pH=14), 3.5 wt% NaCl solution, and ultraviolet. The evaluation resulted of the chemical stability of the coating are shown in Fig. 9.

Fig. 9a,b depicted the changes in wettability of the coating after immersion in acidic (pH=2) and alkaline (pH=14) solutions for different durations. As the immersion time in strong acid (pH=2) and strong alkaline (pH=14) solutions increased, the WCA gradually decreased, and the SA gradually increased. After one day of immersion, both the WCA and SA showed a certain degree of decline, with the WCA remaining above 160° and the SA below 10°. When the coating was immersed for 6 days, there was a significant changes in both WCA and SA, but the WCA still remained above 150°, indicating long-term stability of the coating in strong acid and strong alkaline solutions. This could be attributed to the excellent acid and alkali resistance of SiC, CNTs, and EP. However, it is observed that the coating is more affected by alkaline environments compared to acidic environments. In alkaline solutions, we believed that the Si-O-Si bonds react with OH<sup>-</sup> to form Si-O anionic groups, disrupting the surface rough structure of the coating. This led to a faster decrease in WCA in alkaline environments compared to acidic environments<sup>[30]</sup>. As shown in Fig. 9c, with the increase in immersion time of the coating in a 3.5wt% NaCl solution, the WCA continuously decreased, and the SA increased. However, the WCA remained above 150°, and the SA stayed below 10°, indicating that the coating could withstand the erosion of a 3.5 wt% NaCl solution. As shown in Fig. 9d, the results indicated that with prolonged ultraviolet time, the changes in WCA and SA were not significant. Even after 6 days of ultraviolet, WCA and SA remained at the same level as before the test. The coating demonstrated excellent resistance to ultraviolet.

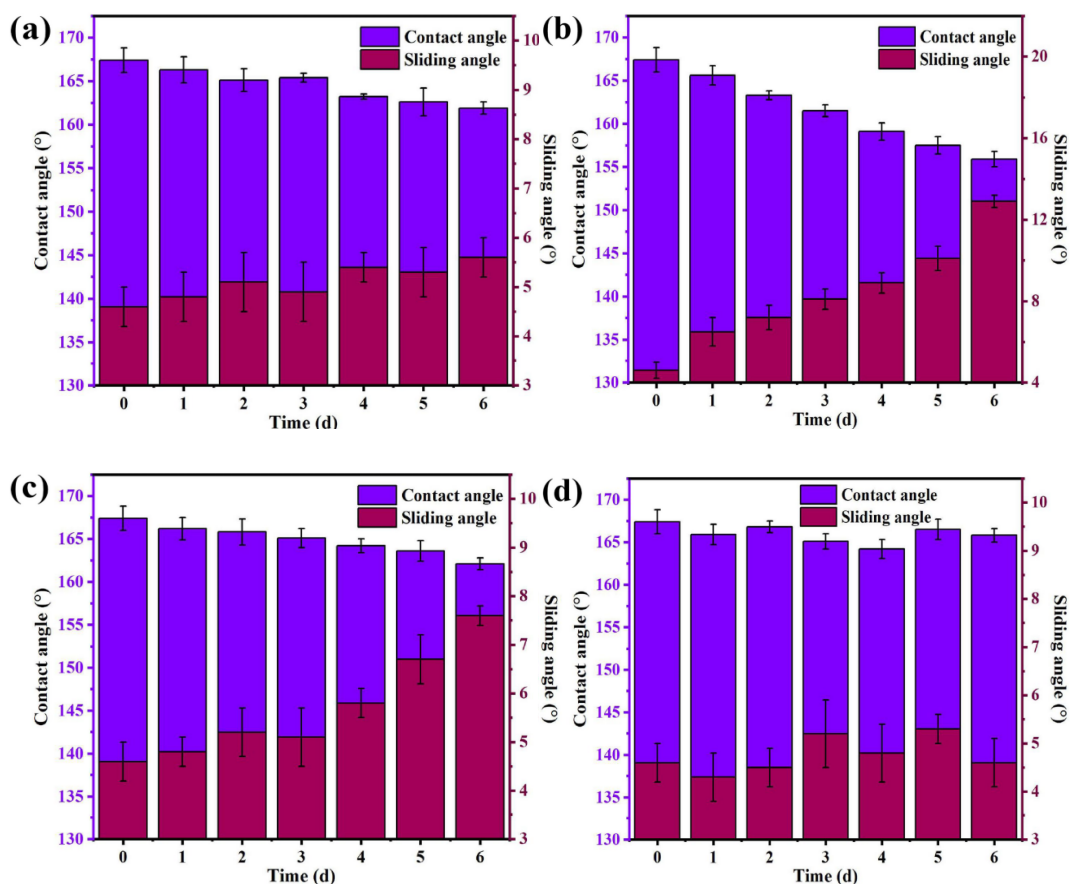


Fig. 9. (a) Variation of the coating surface wettability after immersion in acidic solution (pH=2), (b) Variation of the coating surface wettability after immersion in alkaline solution (pH=14), (c) Variation of the coating surface wettability after immersion in 3.5 wt% NaCl solution, (d) Variation of the coating surface wettability after ultraviolet.

The primary factor contributing to the high chemical stability of the coating is the presence of an air layer within micro-nano pores, which acts as a barrier preventing corrosive ions in the solution from eroding the coating. While the solution may gradually infiltrate the air layer over time, impacting the superhydrophobic properties of the coating, it ultimately does not inflict any damage upon the coating.

To examine the variation in surface wettability of superhydrophobic coatings under high temperatures, the coating was kept at different temperatures for 2 hours, and the results were shown in Fig. 10. It was evident that, although the coating was kept at 100°C, 200°C, and 300°C for 2 h, respectively, the color of the coating remained unchanged. However, when the coating was kept at 400°C for 2 h, the color of the coating changed from black to dark gray. When the coating was further kept at 500°C for 2 h, the color of the coating changed from dark gray to yellowish gray. This may be due to the carbonization of epoxy resin at high temperatures, causing a yellowish color that covered the surface of carbon nanotubes and led to a transformation in the color of the coating. Despite the alteration in color of the coating at elevated temperatures, no cracks or foaming were observed on the coating surface, indicating that the superhydrophobic properties remained unaffected. As shown in Fig. 10f, as the temperature increased, the WCA of the coating remained above 150°, and the SA stayed below 10°. The results suggest that incorporating SiC particles with excellent high-temperature stability into the EP+RTV layer significantly enhanced the high-temperature stability of the coating.

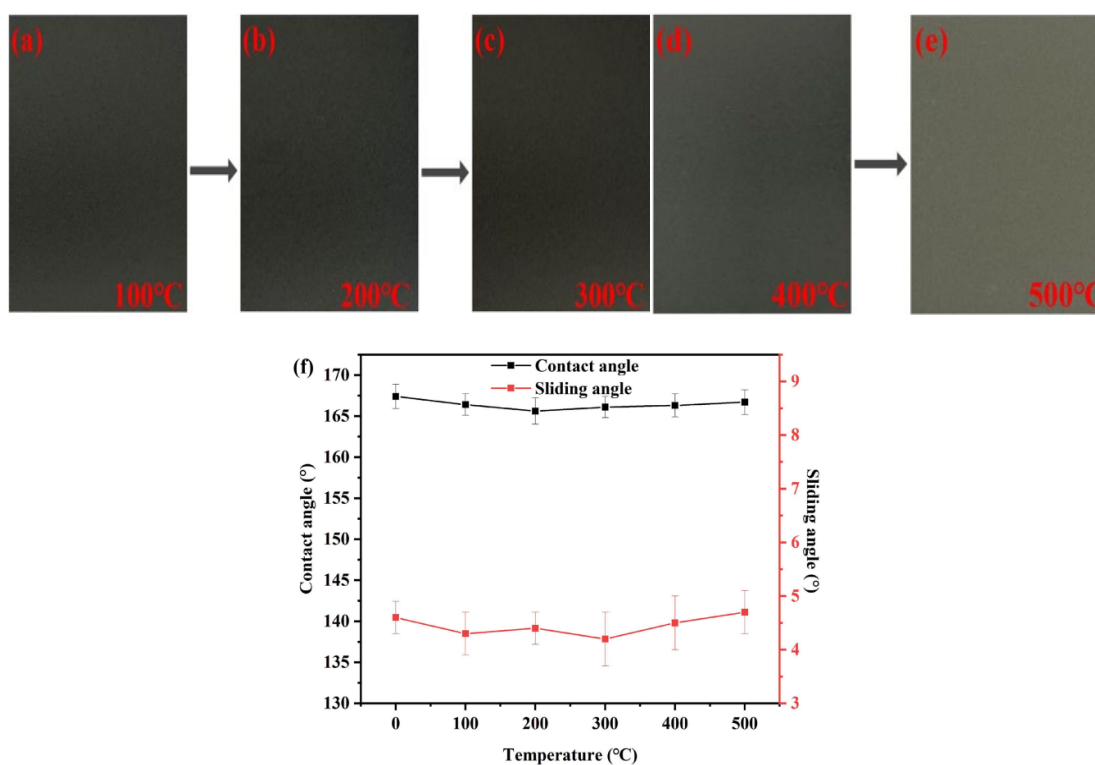


Fig. 10. (a) (b) (c) (d) (e) are the surface appearance of the coatings after being kept at different temperatures for 2 h, (f) is the wettability change of the coating after being kept at different temperatures for 2 h.

### 3.5. Anti-corrosion test

The corrosion resistance of the superhydrophobic coating in a 3.5 wt% NaCl solution was studied through kinetic potential polarization curve. The polarization curves of samples with different treatment processes are shown in Fig. 11. Generally, better corrosion resistance was attributed to lower  $i_{corr}$  (corrosion current) and higher  $E_{corr}$  (corrosion potential). The  $E_{corr}$ ,  $i_{corr}$ , and

corrosion inhibition efficiency calculated by Tafel extrapolation were presented in Table 1. Compared to bare aluminum sheet, the  $E_{corr}$  of the superhydrophobic coating shifted approximately 0.5 V towards the positive direction, and  $i_{corr}$  decreased significantly from  $1.27 \times 10^{-8} \text{ A/cm}^2$  to  $5.49 \times 10^{-12} \text{ A/cm}^2$ , a reduction of about four orders of magnitude. The corrosion inhibition efficiency of the superhydrophobic coating is calculated using the following formula<sup>[42]</sup>:

$$n_p (\%) = \frac{i_{corr}^0 - i_{corr}}{i_{corr}^0} \times 100\% \quad (1)$$

where  $i_{corr}^0$  and  $i_{corr}$  represent the corrosion current density of the coating and untreated aluminum plate, respectively. The calculated corrosion inhibition efficiency was 99.92%. This indicated a significant improvement in the corrosion resistance of the superhydrophobic surface compared to the untreated aluminum sheet surface.

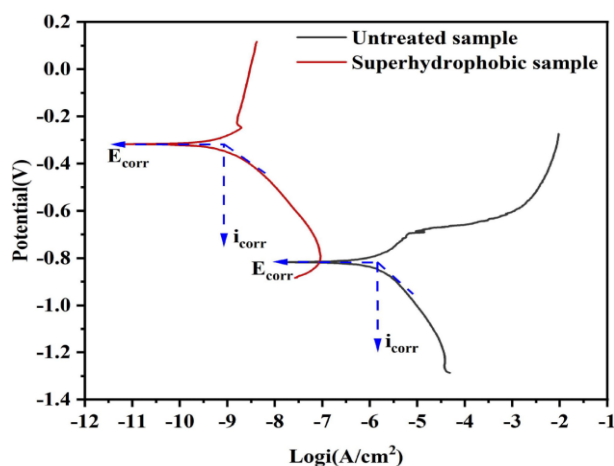


Fig. 11. Kinetic potential polarization curves of untreated and superhydrophobic samples.

Table 1.  $E_{corr}$  and  $i_{corr}$  of untreated aluminum sheet and superhydrophobic coating in 3.5 wt. % NaCl solution.

Sample	$E_{corr}$ (mV)	$i_{corr}$ (A/cm <sup>2</sup> )	$n_p$ (%)
Untreated	-821	$1.27 \times 10^{-8}$	-
Superhydrophobic	-317	$5.49 \times 10^{-12}$	99.92%

Schematic diagrams of different sample surfaces were used to further illustrate the corrosion protection mechanism. For untreated aluminum substrates, due to the absence of a protective layer, Corrosive ions easily corrode the surface of aluminum materials. Therefore, highly corrosive ions directly contact the substrate surface, initiating corrosion reactions and leading to localized corrosion such as pitting and intergranular corrosion (Fig. 12a). In contrast, when the superhydrophobic coating comes into contact with a corrosive solution (Fig. 12b), the porous structure on the superhydrophobic coating surface with micro-nano hierarchical rough structure can capture a significant amount of air, forming a dense air layer that can stably exist for a certain period. This effectively prevents the direct contact between highly corrosive ions and the aluminum sheet, thus blocking the penetration of highly corrosive ions<sup>[43]</sup>. The highly corrosive ions are easily blocked out and cannot directly contact the substrate surface. These results indicate that the superhydrophobic coating plays a crucial role in corrosion protection.

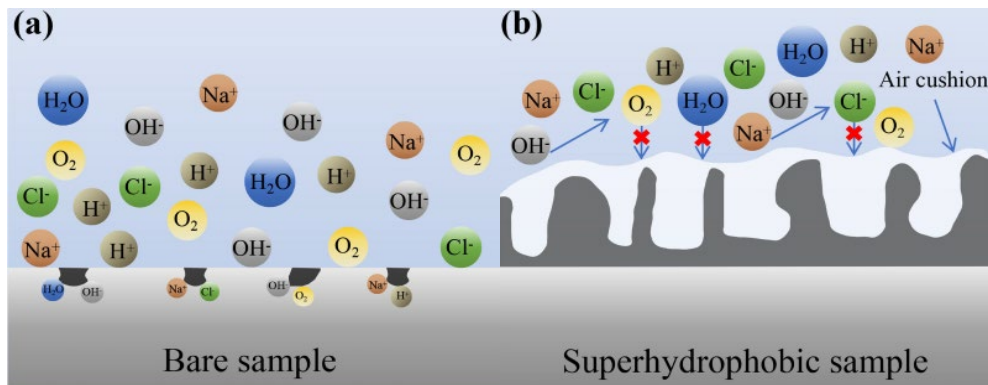


Fig. 12. (a) Schematic diagram of the aluminum sheet surface; (b) Schematic diagram of Superhydrophobic surface.

### 3.5. Anti-icing and de-icing performance tests

The anti-icing performance of the coating is crucial when used outdoors. Fig. 13 showed the images of water droplets in the delayed freezing stage on the surface of bare aluminum sheet (Fig. 13a) and superhydrophobic coating (Fig. 13b) at  $-10\text{ }^{\circ}\text{C}$ .

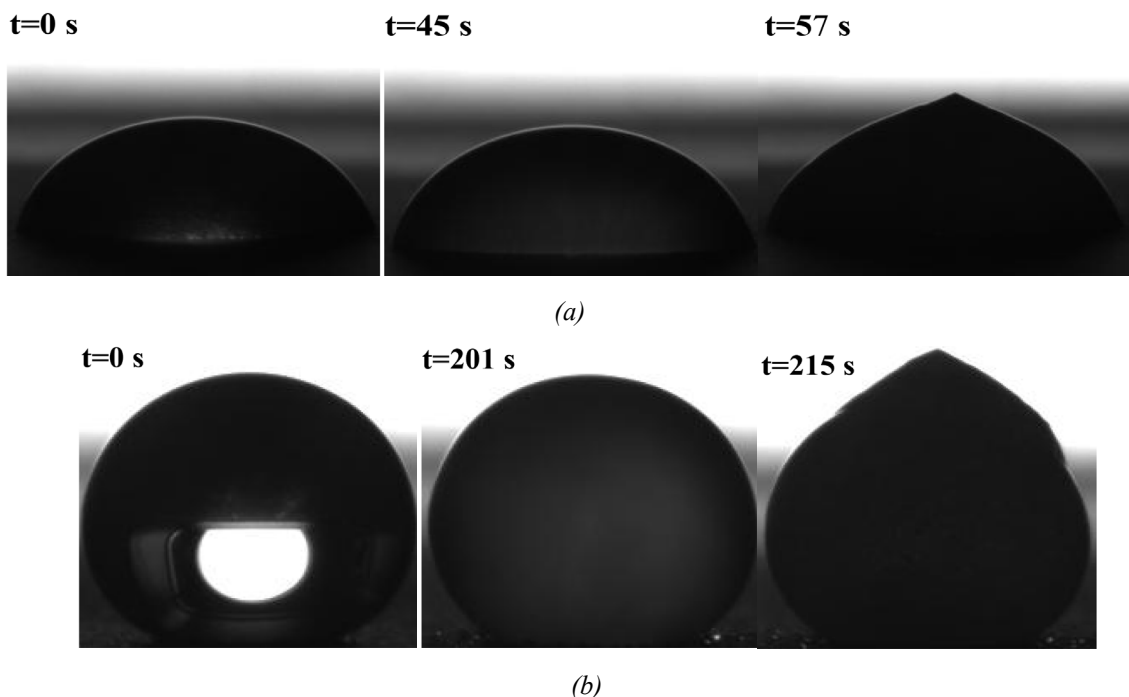
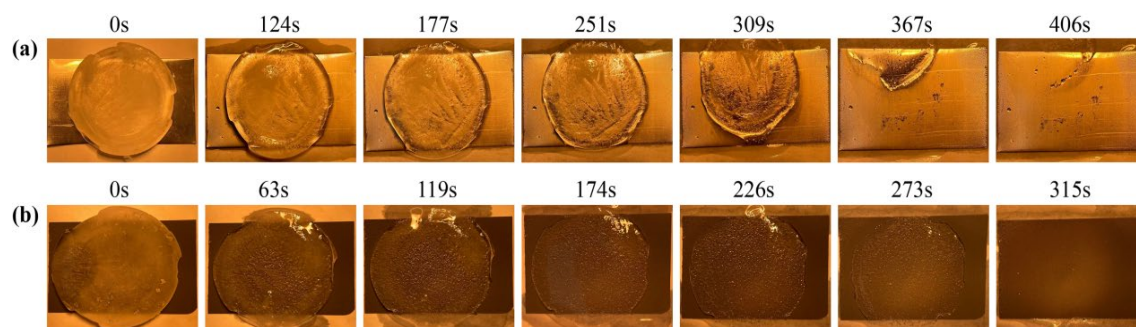


Fig. 13. The freezing process of water droplets at  $-10\text{ }^{\circ}\text{C}$  on the surface of bare aluminum sheets and superhydrophobic surfaces.

It could be clearly observed that the water droplet on the bare aluminum surface was triangular in shape and it began to freeze at 45 s and completely froze at 57 seconds. In contrast, on the superhydrophobic surface, the water droplet maintained spherical, starting to freeze at 201 s and fully freezing at 215 s. During the process of gradual freezing, the circle of light of the water droplet becomes smaller. When the water droplet was completely frozen, the circle of light

disappeared and presented a peach in shape. This shape was formed as the tetrahedral stryctyre formed by water molecules elongate the intermolecular distance[44]. Due to the significantly reduced contact area and heat transfer efficiency between water droplets and the surface, the coating extended the time for water droplets to completely freeze compared to the bare aluminum surface by four times. The coating exhibited outstanding anti-icing capability.

In practical applications, the coating needs to possess both active anti-icing performance and passive anti-icing capabilities[45]. In the passive anti-icing performance test, a bare aluminum sheet and a superhydrophobic coating, both with the same size of ice layer, were placed under a xenon lamp. The xenon lamp was used to simulate solar irradiation. The passive de-icing performance was evaluated by comparing the melting speed of the ice layers on the surface of the two samples. Fig. 14. illustrated the melting process of the ice layers on the surfaces of the bare aluminum sheets and the superhydrophobic coating under xenon lamp irradiation. Under the continuous xenon lamp irradiation, what can be observed was that the melting time of the ice layers on the surface of bare aluminum sheets was 406 s, while the melting time on the superhydrophobic coating surface was 315 s, which was 91 seconds faster than the bare aluminum sheet. This demonstrated excellent de-icing ability. This was attributed to the outstanding photothermal conversion performance of carbon nanotubes, which facilitated the efficient conversion of more light energy into thermal energy, rapidly raising the temperature of the coating surface and allowing the ice layer on the coating surface to melt faster than the ice layer on the bare aluminum sheets surface.



*Fig. 14. (a) is the process of ice layer melting on the surface of bare aluminum sheets under xenon lamp irradiation, (b) is the process of ice layer melting on the surface of superhydrophobic coating under xenon lamp irradiation.*

#### 4. Conclusions

In conclusion, a robust superhydrophobic coating was successfully prepared using a simple spraying method, with SiC particles of different sizes (5 $\mu$ m, 50nm) deposited on the surface. The influence of the mass ratio of  $\mu$ -SiC to n-SiC on the surface morphology and wettability of the coating was investigated. RTV can interacted with EP to enhance the interfacial interaction between micro-nanomaterials and polymers, so that micro-nanoparticles were firmly attached to the substrate, and the superhydrophobic properties were also excellent. This coating can be applied to various substrates, such as board, steel, paper, and glass, with high WCA and low SA. Simultaneously, the coating also exhibited excellent anti-fouling and self-cleaning properties. The coating demonstrated outstanding durability in various harsh environments, withstanding 1000 abrasion cycles, 100 cycles of sand impact, and 60 tape-peeling cycles. The coating demonstrated excellent adhesion in the cross-cut test, reaching the highest grade (Grade 1). The coating exhibited outstanding chemical stability and maintained superhydrophobicity even after immersion in different corrosive solutions for 6 days. When the coating was kept at 500 $^{\circ}$ C for 2 h, the surface color of the coating undergoes some changes, but it still retained its superhydrophobic properties. The corrosion resistance of the superhydrophobic coating in 3.5 wt% NaCl solution was investigated through kinetic potential polarization curve. The corrosion inhibition efficiency of the

coating can reach 99.92%, demonstrating excellent corrosion resistance. The coating also demonstrated excellent photothermal performance, making it suitable for anti-icing/deicing applications. In summary, the prepared superhydrophobic coating was resistant to damage from external environmental factors and exhibited outstanding stability.

### Acknowledgements

This work was supported by the National Natural Science Foundation of China (52073127) and the International Science and Technology Cooperation Project of Changzhou Science and Technology Bureau (CZ20230024).

### References

- [1] P. Wang, C.Y. Li, D. Zhang, *Journal of Materials Science & Technology*, 2022, 129: 40-69; <https://doi.org/10.1016/j.jmst.2022.01.045>
- [2] W.L. Li, Y.K. Zong, Q. Liu, Y. Sun, Z.R. Li, H.P. Wang, Z.X. Li, *A Progress in Organic Coatings*, 2020, 147: 105776; <https://doi.org/10.1016/j.porgcoat.2020.105776>
- [3] B.F. Li, X.X. Yin, S.Y. Xue, P. Mu, J. Li, *Applied Surface Science*, 2022, 580: 152305; <https://doi.org/10.1016/j.apsusc.2021.152305>
- [4] B.B. Zhang, W.C. Xu, Coninck.J.De, et al., *New Journal of Chemistry*, 2021, 45: 15170-15179; <https://doi.org/10.1039/D1NJ03158A>
- [5] H. Li, X.L. Feng, Y.J. Peng, R.C. Zeng, *Nanoscale*, 2020, 12: 7700-7711; <https://doi.org/10.1039/C9NR10699E>
- [6] F. Xiao, H.X. Zhang, T.Z. Wu, J.H. Liu, J.X. Liu, J.B. Zhang, W. Liu, T.X. Liang, J.H. Hu, *Process Safety and Environmental Protection*, 2022, 161: 13-21; <https://doi.org/10.1016/j.psep.2022.01.043>
- [7] S.F. Zhang, S.P. Chen, H.Q. Li, X.J. Lai, X.R. Zeng, *Journal of Environmental Chemical Engineering*, 2022, 10: 107580; <https://doi.org/10.1016/j.jece.2022.107580>
- [8] X.D. Chen, L. Hu, Y.Z. Du, *Materials Chemistry and Physics*, 2022, 291: 126683; <https://doi.org/10.1016/j.matchemphys.2022.126683>
- [9] Y.M. Jian, H.T. Gao, Y.Y. Yan, *Colloids and Surfaces A: Physicochemical and Engineering Aspects*, 2022, 651: 129761; <https://doi.org/10.1016/j.colsurfa.2022.129761>
- [10] L.H. Kong, *Surface & Coatings Technology*, 2021, 407: 126777; <https://doi.org/10.1016/j.surfcoat.2020.126777>
- [11] X.Q. Fan, S.J. Song, Y.T. Shi, M. Cai, Y. Huang, B.B. Zhang, M.H. Zhu, *Progress in Organic Coatings*, 2023, 178: 107478; <https://doi.org/10.1016/j.porgcoat.2023.107478>
- [12] T.P. Rasitha, S.C. Vanithakumari, D.N.G. Krishna, R.P. George, R. Srinivasan, J. Philip, *Progress in Organic Coatings*, 2022, 162: 106560; <https://doi.org/10.1016/j.porgcoat.2021.106560>
- [13] W.T. Hao, Q.N. Zheng, Y.N.J. Zhong, X.K. Meng, H.L. Wang, L.Z. Qiu, H.B. Lu, Y.P. Huang, W. Yang, *Progress in Organic Coatings*, 2023, 185: 107892; <https://doi.org/10.1016/j.porgcoat.2023.107892>
- [14] T.L. Sun, L. Feng, X.F. Gao, L. Jiang, *Accounts of Chemical Research*, 2005, 38(8): 644-652; <https://doi.org/10.1021/ar040224c>

- [15] Z.H. Wang, L. Yuan, G.Z. Liang, A.J. Gu, *Chemical Engineering Journal*, 2021, 408: 127623; <https://doi.org/10.1016/j.cej.2020.127263>
- [16] G.J. Li, B. Jiang, H.Q. Liu, L. N, D.Q. Yi, X.M. Wang, Z.Y. Liu, *Progress in Organic Coatings*, 2019, 137: 105315; <https://doi.org/10.1016/j.porgcoat.2019.105315>
- [17] N. Ma, D. Cheng, J.Q. Zhang, S.G. Zhao, Y. Lu, *Surface & Coatings Technology*, 2020, 399: 126180; <https://doi.org/10.1016/j.surfcoat.2020.126180>
- [18] C. Ke, C.H. Zhang, X.G. Wu, Y.D. Jiang, *Thin Solid Films*, 2021, 723: 138583; <https://doi.org/10.1016/j.tsf.2021.138583>
- [19] Y.Q. Qing, C. Long, K. An, C.B. Hu, C.S. Liu, *Journal of Colloid and Interface Science*, 2019, 548: 224-232; <https://doi.org/10.1016/j.jcis.2019.04.040>
- [20] J.Z. Sun, Q.C. Zhang, Y.S. Jiang, H. Li, B.B. Zhang, *Colloids and Surfaces A: Physicochemical and Engineering Aspects*, 2023, 658: 130702; <https://doi.org/10.1016/j.colsurfa.2022.130702>
- [21] G. Barati Daraband, M. Aliofkhaezrai, S. Khorsand, S. Sokhanvar, A. Kaboli, *Arabian Journal of Chemistry*, 2020, 13: 1763-1802; <https://doi.org/10.1016/j.arabjc.2018.01.013>
- [22] W.L. Zhang, D.H. Wang, Z.N. Sun, J.N. Song, X. Deng, *Chemical Society Reviews*, 2021, 50: 4031-4061; <https://doi.org/10.1039/D0CS00751J>
- [23] J. X, J. Hu, X.D. Lin, L. Fang, F. Wu, X.L. Liao, H.J. Luo, L.T. Shi, *Applied Surface Science*, 2018, 457: 870-880; <https://doi.org/10.1016/j.apsusc.2018.06.250>
- [24] Y.H. Xiu, Y. Liu, D.W. Hess, C.P. Wong, *Nanotechnology*, 2010, 21: 155705; <https://doi.org/10.1088/0957-4484/21/15/155705>
- [25] P. Zhu, L.J. Zhu, F.F. Ge, G. Wang, Z.X. Zeng, *Surface & Coatings Technology*, 2022, 443: 128609; <https://doi.org/10.1016/j.surfcoat.2022.128609>
- [26] Z. Xiao, Q.L. Wang, D.Z. Yao, X.Q. Yu, Y.F. Zhang, *Langmuir*, 2019, 35(20): 6650-6656; <https://doi.org/10.1021/acs.langmuir.9b00690>
- [27] M. Aliakbari, O.M. Jazabi, M. Sohrabian, M. Jouyandeh, M.R. Saeb, *Progress in Organic Coatings*, 2019, 133: 376-386; <https://doi.org/10.1016/j.porgcoat.2019.04.076>
- [28] Y. Huangfu, C.B. Liang, Y.X. Han, H. Qiu, P. Song, L. Wang, J. Kong, J.W. Gu, *Composites Science and Technology*, 2019, 169: 70-75; <https://doi.org/10.1016/j.compscitech.2018.11.012>
- [29] M.Y. Li, N. Liu, J.H. Chen, Q.L. Li, *Journal of the Taiwan Institute of Chemical Engineers*, 2019, 95: 682-691; <https://doi.org/10.1016/j.jtice.2018.10.016>
- [30] Z. Hong, H.W. Jiang, M.S. Xue, C.Y. Ke, Y.D. Luo, Z.Z. Yin, C. Xie, F. Zhang, Y. Xing, *Progress in Organic Coatings*, 2022, 168: 106909; <https://doi.org/10.1016/j.porgcoat.2022.106909>
- [31] N. Domun, H. Hadavinia, T. Zhang, T. Sainsbury, G.H. Liaghat, S. Vahid, *Nanoscale*, 2015, 7: 10294-10329; <https://doi.org/10.1039/C5NR01354B>
- [32] H.J. Qian, M.L. Zhu, H. Song, H.Y. Wang, Z.J. Liu, C.J. Wang, *Progress in Organic Coatings*, 2020, 142: 105566; <https://doi.org/10.1016/j.porgcoat.2020.105566>
- [33] G. Momen, M. Farzaneh, R. Jafari, *Applied Surface Science*, 2011, 257: 6489-6493; <https://doi.org/10.1016/j.apsusc.2011.02.049>
- [34] G. Wen, J.X. Huang, Z.G. Guo, *Colloids and Surfaces A*, 2019, 568: 20-28; <https://doi.org/10.1016/j.colsurfa.2019.01.067>
- [35] Q. Li, Z.G. Guo, *Journal of Materials Chemistry A*, 2018, 6: 13549-13581;

<https://doi.org/10.1039/C8TA03259A>

- [36] X. Shen, T.C. Mao, C.Q. Li, F.F. Mao, Z.Y. Xue, G.Q. Xu, A. Amirfazli, Durable superhydrophobic coatings based on CNTs-SiO<sub>2</sub>gel hybrids for anti-corrosion and thermal insulation, 2023, 181: 107602; <https://doi.org/10.1016/j.porgcoat.2023.107602>
- [37] T.C. Mao, C.Q. Li, F.F. Mao, Z.Y. Xue, G.Q. Xu, A. Amirfazli, Diamond and Related Materials, 2022, 129: 109370; <https://doi.org/10.1016/j.diamond.2022.109370>
- [38] P.Y. Xu, T.W. Coyle, L. Pershin, J. Mostaghimi, Materials and Design, 2018, 160: 974-984; <https://doi.org/10.1016/j.matdes.2018.10.015>
- [39] J.X. Zhang, L.G. Zhang, X. Gong, Langmuir, 2021, 37: 6042-6051; <https://doi.org/10.1021/acs.langmuir.1c00706>
- [40] C.H. Xue, H.D. Wang, Z.Y. Ji, X.J. Guo, B.Y. Liu, Y. Wu, S.T. Jia, ACS Omega, 2019, 4(22): 19756-19764; <https://doi.org/10.1021/acsomega.9b02535>
- [41] B. Swain, S.K. Bhuyan, S.S. Mohapatra, D.K. Rajak, A. Behera, C.I. Pruncu, Engineering Failure Analysis, 2022, 140: 106368; <https://doi.org/10.1016/j.engfailanal.2022.106368>
- [42] B. Han, H.Y. Wang, S.C. Yuan, Y. Li, X.G. Zhang, D. Lin, L. Chen, Y.J. Zhu, Progress in Organic Coatings, 2020, 149: 105922; <https://doi.org/10.1016/j.porgcoat.2020.105922>
- [43] H.J. Cao, Colloids and Surfaces A: Physicochemical and Engineering Aspects, 2022, 652: 129893; <https://doi.org/10.1016/j.colsurfa.2022.129893>
- [44] J. Li, Y. Zhou, W. Wang, C. Xu, L. Ren, Langmuir, 2020, 36: 1075-1082; <https://doi.org/10.1021/acs.langmuir.9b02273>
- [45] Z.Y. Liu, J.H. Hu, G. Jiang, Surface & Coatings Technology, 2022, 444: 128668; <https://doi.org/10.1016/j.surfcoat.2022.128668>